A virus-encoded protein suppresses methylation of the viral genome through its interaction with AGO4 in the Cajal body

Liping Wang[1,2], Yi Ding[1,2], Li He[1], Guiping Zhang[1], Jian-Kang Zhu[1], Rosa Lozano-Duran[1]

[1]Shanghai Center for Plant Stress Biology, Chinese Academy of Sciences, Shanghai 201602, China; Center for Excellence in Molecular Plant Science, Chinese Academy of Sciences. [2]University of the Chinese Academy of Sciences, Beijing 100049, China

ABSTRACT

DNA methylation is a eukaryotic anti-viral defence mechanism. In plants, establishment of *de novo* DNA methylation is regulated by the RNA-directed DNA methylation pathway, which requires AGO4 function. The genome of the plant DNA viruses geminiviruses replicates in the nuclei of infected cells through not yet fully understood mechanisms and is subjected to methylation, a modification that negatively impacts infectivity. In *Tomato yellow leaf curl virus*, the virus-encoded V2 protein suppresses methylation of the viral DNA. Here, we identify AGO4 as a physical interactor of V2. AGO4 mediates methylation of the viral genome, which is countered by V2. Accordingly, virulence of a V2 mutant virus is partially restored by *AGO4* silencing, hinting at the inhibition of AGO4 as a crucial virulence function of V2. Virus-produced V2 does not affect accumulation of viral small interfering RNA nor prevents their loading into AGO4, but impairs binding of this protein to the viral DNA. Importantly, the association between V2 and AGO4 occurs in the Cajal body, uncovering this subnuclear compartment as a crucial site in the viral cycle.

Running title: V2 inhibits AGO4 in the Cajal body

Keywords: Geminivirus, AGO4, Cajal body, DNA methylation, virus.

INTRODUCTION

DNA methylation in cytosine residues is a conserved epigenetic mark essential for protecting the eukaryotic genome against invading nucleic acids, namely viruses and transposable elements. In plants, establishment of *de novo* DNA methylation is believed to be regulated by the RNA-directed DNA methylation (RdDM) pathway. The canonical RdDM pathway requires the activity of two plant-specific RNA polymerase II-related enzymes, Pol IV and Pol V, and leads to cytosine methylation in a sequence-specific manner. In brief, the current understanding of RdDM is as follows: Pol IV generates RNA transcripts subsequently converted to double-stranded RNA (dsRNA) by RDR2 (Haag et al., 2012, Law et al., 2011), and then diced into 24-nt siRNAs by DCL3 (Xie et al., 2004); the resulting 24-nt siRNAs are loaded into AGO4 (Zilberman et al., 2003), which is guided to scaffold RNA molecules generated by Pol V via sequence complementarity and recruits the *de novo* methyl transferase DRM2 (Böhmdorfer et al., 2014, Chan et al., 2005, Gao et al., 2010, Zhong et al., 2014), which in turn catalyses methylation of adjacent DNA sequences. RdDM generally creates a chromatin environment refractive to gene expression.

Geminiviruses are a family of plant viruses with circular single-stranded (ss) DNA genomes infecting multiple crops and causing dramatic yield losses worldwide. The geminiviral genome replicates in the nucleus of the infected cell by using the host DNA replication machinery, made available following the viral re-programming of the cell cycle (reviewed in Hanley-Bowdoin et al., 2013). During viral multiplication, the ssDNA genome generates a double-stranded (ds) DNA intermediate, which then undergoes rolling-circle replication (reviewed in Hanley-Bowdoin et al., 2013). However, the cellular and molecular details underlying these essential initial steps of the viral infection cycle, including the subnuclear localization of viral ss and ds DNA accumulation and of the processes leading to their production, are to date mostly unknown.

Notably, the geminiviral genome forms minichromosomes and is subjected to epigenetic modifications, including cytosine DNA methylation and histone modifications (Ceniceros-Ojeda et al., 2016, Deuschle et al., 2016, Jackel et al., 2016, Kushwaha et al., 2017, Raja et al., 2008, Wang et al., 2018). The findings that methylation of viral DNA negatively impacts viral replication (Brough et al., 1992, Ermak et al., 1993), that different geminivirus-encoded proteins have evolved to suppress DNA methylation (Buchmann et al., 2009, Ismayil et al., 2018, Raja et al., 2008, Rodriguez-Negrete et al., 2013, Tu et al., 2017, Wang et al., 2018, Yang et al., 2013, Yang et al., 2011, Zhang et al., 2011), and that methylation of the viral genome correlates with host resistance or recovery (Butterbach et al., 2014, Ceniceros-Ojeda et al., 2016, Raja et al., 2008, Torchetti et al., 2016, Yadav & Chattopadhyay, 2011) strongly support the idea that the plant-mediated

methylation of the viral DNA acts as an anti-viral defence mechanism, underscoring DNA methylation as an active plant-virus battlefield.

During the infection by the geminivirus *Tomato yellow leaf curl virus* (TYLCV), the essential virus-encoded protein V2 has been shown to suppress DNA methylation of the viral genome (Wang et al., 2014). V2 interacts with the histone deacetylase HDA6 in *Nicotiana benthamiana*, competing with the recruitment of the maintenance CG methyltransferase MET1 (Woo et al., 2008) and ultimately reducing viral DNA methylation (Wang et al., 2018). However, silencing of *HDA6* results in limited complementation of a V2 null mutation in the virus and in only a partial reduction in viral DNA methylation (Wang et al., 2018), suggesting that V2 might counter methylation through additional interactions with host factors.

In this work, we show that V2 from TYLCV interacts with the central RdDM component AGO4; that AGO4 plays a role in anti-TYLCV defence; and that V2 and AGO4 have opposite effects on the methylation of the viral genome. Our results indicate that the viral DNA gets methylated in the absence of V2, and that increased methylation and reduced accumulation of a V2-defective virus can be countered by silencing of *AGO4*. The presence of V2 does not affect production of viral small interfering RNAs (vsiRNA) or prevent their loading into AGO4, but impairs binding of this protein to the viral genome. Importantly, the physical interaction between V2 and AGO4 occurs mostly in the Cajal body, unveiling this subnuclear compartment as a crucial site in the viral cycle and in anti-viral DNA methylation. In summary, this work not only describes AGO4 as a target of the viral suppressor of DNA methylation V2, but also hints at a functional relevance of subnuclear compartmentalization of viral processes and components, and suggests a prominent role of the Cajal body in the viral infection.

RESULTS

V2 from TYLCV interacts with AGO4 from *Nicotiana benthamiana* and tomato in the Cajal body

With the aim of gaining insight into the functions of V2 from TYLCV in the plant cell, we used transient expression of GFP-tagged V2 in infected leaf patches of *N. benthamiana* followed by affinity purification and mass spectrometry (AP-MS) to identify plant interactors of this viral protein in the context of the infection (Wang et al., 2017a). Interestingly, we identified the two AGO4 paralogs in *N. benthamiana* (NbAGO4-1 and NbAGO4-2) as associated to V2-GFP (Figure 1A;

Wang et al., 2017a); these interactions were confirmed by co-immunoprecipitation and split-luciferase assays (Figure 1B,C).

There are four *AGO4* orthologues in tomato (*SlAGO4a-d*) (Bai et al., 2012), the natural and economically relevant host of TYLCV (Figure 2A,B). All four SlAGO4-encoding genes are expressed in basal conditions in tomato leaves, although *SlAGO4c* and *d* show low expression levels; *SlAGO4b*, *c*, and *d* are slightly up-regulated by TYLCV infection (Supplementary figure 1). *SlAGO4a*, *SlAGO4b*, and *SlAGO4d* were cloned and the encoded proteins confirmed as interactors of V2 in co-IP and split-luciferase assays (Figure 2C,D).

In Arabidopsis, AGO4 has been shown to co-localize with its interactor NRPE1 (NRPD1b), a subunit of Pol V, in the Cajal body, which was then suggested to be a center for the assembly of AGO4/NRPE1/siRNA complexes, enabling RdDM at target loci (Li et al., 2008, Li et al., 2006). Interestingly, both V2-GFP and the different RFP-AGO4 orthologues from *N. benthamiana* and tomato co-localize in a distinct subnuclear compartment, identified as the Cajal body by the accumulation of the nucleolus and Cajal body marker fibrillarin (Barneche et al., 2000), upon transient expression in *N. benthamiana* (Figure 3A). Of note, most of nuclear V2-GFP accumulates in the Cajal body, although some fluorescence can be detected in the nucleoplasm. All AGO4 orthologues are distributed throughout the nucleoplasm and absent from the nucleolus; clear Cajal body localization can be detected for NbAGO4-1, NbAGO4-2, SlAGO4a, and SlAGO4b, while Cajal body localization of SlAGO4d is less conspicuous (Figure 3A). Analysis of the V2/AGO4 interaction by bimolecular fluorescence complementation (BiFC), which is based on visualization and hence provides spatial information, unveiled that, strikingly, the association between these two proteins occurs mostly or exclusively in the Cajal body, where V2 homotypic interactions also occur (Figure 3B).

V2 counters the AGO4-dependent methylation of the viral genome to promote virulence

In order to evaluate the contribution of V2 to the viral infection, we generated an infectious TYLCV clone carrying a G-to-A mutation in the fifth nucleotide of the V2 open reading frame (ORF), which converts the second codon (encoding tryptophan) to a stop codon (Supplementary figure 2A), making it unable to produce the V2 protein (TYLCV-V2null). In agreement with previous results (Wartig et al., 1997), V2 is required for full infectivity in both tomato and *N. benthamiana*, since the V2 null mutant accumulates to very low levels and produces no noticeable symptoms (Supplementary figure 2).

Next, we sought out to test whether knock-down of *AGO4* could partially complement the lack of V2 during the TYLCV infection. For this purpose, we employed virus-induced gene silencing (VIGS) to silence both *NbAGO4-1* and *NbAGO4-2.* VIGS efficiently knocked-down both *NbAGO4* orthologues, but did not affect accumulation of the transcript of the close homologue *NbAGO6* (Figure 4A); AGO4-silenced plants did not display any obvious developmental abnormalities (Figure 4B). Expression of *NbAGO4-1* or *NbAGO4-2* was not affected by TYLCV infection, neither in silenced nor in non-silenced plants (Figure 4C,D). Mutation in V2 does not affect viral replication (Wartig et al., 1997), and therefore viral accumulation in local infections in *N. benthamiana* (leaf patch agroinfiltration assays; see Supplementary figure 3) was not different between the WT virus and the V2 null mutant virus (Figure 4E); in both cases, *AGO4* silencing led to a slight increase in viral accumulation, suggesting an anti-viral role for AGO4 (Figure 4E). Interestingly, in systemic infections (see Supplementary figure 3), *AGO4* silencing mildly increased viral accumulation of the WT TYLCV (1.33-fold), but dramatically improved performance of the V2 null mutant virus (3.23-fold), suggesting that one of the main roles of V2 during the viral infection is the suppression of AGO4 function (Figure 4F).

In light of the role of AGO4 in RdDM and to directly assess the impact of V2 and AGO4 on the methyl-state of the viral DNA, we used bisulfite sequencing (BS-seq) to measure DNA methylation of the intergenic region of the viral genome, which presents the highest methylation levels during the infection (Piedra-Aguilera et al., 2019). As shown in Figure 5A, cytosine methylation in this region in all contexts (CG, CHG, and CHH) was almost undetectable in the WT viral genome in local infections at 3 or 9 days post-inoculation (dpi), while it reached ~60% and ~80%, respectively, in the V2 null mutant (Figure 5A; Supplementary figure 4). These results indicate that V2 can prevent or revert methylation of the viral genome during the infection, which occurs rapidly in the absence of this protein.

We then compared the percentage of cytosine methylation in the intergenic region in local infections with the V2 null mutant TYLCV in basal conditions or upon *AGO4* silencing. Strikingly, *AGO4* silencing resulted in a ~23% decrease in the percentage of methylated cytosines in all contexts (Figure 5B; Supplementary figure 5), indicating that knock-down of *AGO4* can partially complement the lack of V2 at the level of the viral methylation state. This complementation suggests that a) methylation of the viral DNA at least partially depends on AGO4 function; and b) V2 can at least partially counter AGO4-dependent methylation of the viral DNA.

As opposed to short-timed local infections, in systemic infections in *N. benthamiana*, which require longer timespans and involve viral cell-to-cell and long-distance movement, methylation of the

157 WT viral genome could be detected at ~15% decrease in all contexts (Figure 5C; Supplementary
158 figure 6). Interestingly, the methylation level tends to decrease upon *AGO4* silencing; this
159 reduction (~22%) is more prominent in the V2 null mutant genome, again supporting the idea that
160 AGO4-dependent methylation of the viral genome occurs during the infection and is partially
161 countered by V2. Notably, the detected decrease in methylation correlates with the enhanced
162 viral accumulation in the *AGO4*-silenced plants (Figure 4F).

163

164 **V2 does not hamper production or loading of vsiRNA but interferes with AGO4 binding to**
165 **the viral genome**

166 The canonical function of AGO4 in the RdDM pathway requires loading of siRNA and association
167 to Pol V, and results in the recruitment of DRM2 to the target loci and the subsequent methylation
168 of the adjacent DNA (Matzke et al., 2015, Matzke & Mosher, 2014). Through physical interaction,
169 V2 could affect AGO4 function on the viral genome in different ways, for example by impairing
170 loading of viral siRNA (vsiRNA) onto this protein or by displacing endogenous interactors, such
171 as Pol V or DRM2; our previous results demonstrate that V2 does not affect AGO4 accumulation
172 or localization (Figures 1 and 2). In order to shed light on the molecular mechanism underlying
173 the V2-mediated interference of AGO4-dependent methylation of the viral genome, we tested
174 binding of AGO4 to the viral DNA in the presence or absence of V2 in local infections with TYLCV
175 WT and V2 null mutant, respectively, by Chromatin immunoprecipitation (ChIP). As shown in
176 Figure 6A, 3xFLAG-NbAGO4 could bind both the intergenic (IR) and the V2-encoding region of
177 the viral genome in the absence of V2 (TYLCV-V2null), but the signal decreased to background
178 levels when V2 was present (TYLCV). Therefore, AGO4 has the capacity to bind the viral DNA
179 molecule, but this binding is impaired by the virus-encoded V2 protein. AGO4 binding in the
180 TYLCV V2 null mutant hence correlates with the detected increase in viral DNA methylation
181 (Figure 5A).

182 Several viral silencing suppressors encoded by different viruses have been shown to inhibit
183 formation of AGO/sRNA complexes (e.g. Burgyán et al., 2011, Rawlings et al., 2011, Schott et al.,
184 2012). To test whether this strategy is also employed by V2, we immunoprecipitated 3xFLAG-
185 NbAGO4 co-expressed with WT or V2 null mutant TYLCV in local infection assays in *N.*
186 *benthamiana*, and visualized AGO4-bound vsiRNA by sRNA northern blotting. While infected
187 samples contained both 21- and 24-nt vsiRNA, and the occurrence and accumulation of these
188 sRNA species was not affected by the presence of virus-encoded V2, mostly 24-nt vsiRNA co-

189 immunoprecipitated with AGO4 (Figure 6B). Interestingly, a higher amount of vsiRNA associated
190 to AGO4 in the samples infected with the WT virus (Figure 6B). Taken together, these results
191 demonstrate that V2 does not affect the production or accumulation of vsiRNA, nor does it hamper
192 loading of these vsiRNA molecules into AGO4, but interferes with binding of this protein to the
193 viral genome in order to suppress DNA methylation and promote virulence.

194

195 **DISCUSSION**

196 The plant DNA viruses geminiviruses and pararetroviruses are both targets and suppressors of
197 DNA methylation; this possibly extends to the third family of plant DNA viruses, nanoviruses,
198 although experimental evidence is lacking (reviewed in Poogin, 2013; Pumplin and Voinnet, 2013).
199 The independent evolution of viral suppressors of DNA methylation argues for an anti-viral effect
200 of this epigenetic modification. Indeed, seminal experiments by Brough et al. (1992) and Ermak
201 et al. (1993) demonstrated that methylation of the geminivirus genome interferes with its
202 replication in transformed protoplasts, likely due to a dual effect on viral gene expression and
203 function of the replication complex. More specifically, RdDM seems to play a prominent role in
204 plant defence against geminiviruses, since RdDM mutants or silenced plants display increased
205 susceptibility to geminivirus infection (Raja et al., 2008, Zhong et al., 2017), and DNA methylation
206 and repressive histone marks typical of RdDM are deposited on the viral genome (Castillo-
207 Gonzalez et al., 2015, Ceniceros-Ojeda et al., 2016, Coursey et al., 2018, Dogar et al., 2006,
208 Jackel et al., 2016, Kushwaha et al., 2017, Wang et al., 2018).

209 AGO4 is a central component of the canonical RdDM pathway, and as such an obvious target for
210 viral inhibition. However, AGO4 also affects susceptibility to RNA viruses and viroids, and is
211 targeted by proteins encoded by RNA viruses, which raises the idea that either RdDM on the host
212 genome plays a role in modulating plant-virus interactions broadly, or AGO4 has an anti-viral role
213 beyond RdDM (Brosseau et al., 2016, Ma et al., 2015, Minoia et al., 2014). Supporting the latter,
214 AGO4-dependent defences against a potexvirus are independent of other RdDM components
215 and do not require nuclear localization of AGO4 (Brosseau et al., 2016).

216 The geminivirus TYLCV encodes the essential, multifunctional V2 protein, which acts as a
217 suppressor of viral DNA methylation (Wang et al., 2014). Here, we show that V2 binds to the plant
218 AGO4 in the Cajal body, and suppresses the AGO4-dependent methylation of the viral genome
219 (Figures 1,2,3,5) and the AGO4-mediated restriction of viral accumulation (Figure 4E,F). Our
220 results indicate that AGO4-dependent methylation of viral DNA occurs quickly in the absence of

V2 (Figure 5A,B). Nevertheless, *AGO4* silencing still has a detectable, if minor, positive impact on the accumulation of the WT virus, which correlates with decreased viral DNA methylation (Figure 4E,F; Figure 5C), suggesting that the V2-mediated suppression of AGO4 function is not complete. On the other hand, WT levels of viral DNA methylation are not restored in the V2 mutant upon *AGO4* silencing, which raises the idea that AGO4 might not be the only methylation-related target of V2. In agreement with this, V2 has been shown to bind HDA6 and interfere with its promotion of MET1-dependent methylation of the viral DNA (Wang et al., 2018).

Recently, V2 encoded by the geminivirus *Cotton leaf curl Multan virus* (CLCuMV) was found to interact with AGO4 in *N. benthamiana*, leading to enhanced viral accumulation and a reduction in viral DNA methylation (Wang et al., 2019). It should be noted that the V2 proteins encoded by CLCuMV and TYLCV are only 65% identical (Supplementary figure 7A), and they might have evolved independently to target AGO4. Supporting this notion, mutation of a conserved residue, L76, abolishes the interaction between CLCuMV V2 and NbAGO4 (Wang et al., 2019), but does not affect the interaction between TYLCV V2 and NbAGO4 or SlAGO4, which still occurs in the Cajal body (Supplementary figure 7). This mutation, however, negatively affects V2 self-interaction in the Cajal body (Supplementary figure 7).

The finding that the physical association between TYLCV V2 and AGO4 takes places in a specific nuclear body, the Cajal body, and has an impact on the methyl-state of the viral population in the cell, suggests that all or most viral DNA molecules must localize in this subnuclear compartment at some point of the viral cycle. This observation hints at a functional role of the Cajal body during the infection; whether such a role is linked to gene expression, DNA replication, or some other process remains to be investigated. Interestingly, the Cajal body has been connected to systemic infection of plant RNA viruses, and proteins encoded by RNA viruses can bind coilin, the signature protein of this compartment, which impacts plant-virus interactions (Kim et al., 2007a, Kim et al., 2007b, Semashko et al., 2012, Shaw et al., 2014).

Based on our results, we propose a scenario in which V2 is required to interfere with AGO4 binding to the viral genome, impairing DNA methylation and promoting viral accumulation; whether this effect is linked to the canonical RdDM pathway will require further investigation. In the context of the arms race between host and virus, TYLCV has evolved V2 to target AGO4, impairing its association to the viral DNA and hence suppressing methylation of the viral genome and promoting virulence (Supplementary figure 8). Although the exact molecular mechanism underlying this function of V2 is at present unknown, we hypothesize that the virus-encoded protein might mask a surface required for AGO4 recruitment to the viral DNA through the

association with an endogenous interactor (e.g. NRPE1; Li et al., 2006), or interfere with the complementarity-based pairing to the nascent Pol V transcript. Further work will be necessary to fully elucidate the connections between the Cajal body, DNA methylation, and the geminiviral infection.

MATERIALS AND METHODS

Plasmids and cloning

To generate binary vectors to express *AGO4* from *N. benthamiana* and tomato (cv. Money maker), the full-length coding sequence of *AGO4* genes was amplified using cDNA as template. *NbAGO4-1*, *NbAGO4-2*, *SlAGO4a*, *SlAGO4b*, *SlAGO4d,* and *SlWRKY75* were cloned into pENTR-D/TOPO (Invitrogen) following the manufacturer's instructions. The binary plasmids to express RFP and 3xHA N-terminal fusions were generated by Gateway cloning the AGO4 coding sequence into pGWB555 and pGWB515, respectively (Nakagawa et al., 2007). V2-GFP and the TYLCV infectious clone have been previously described (Rosas-Diaz et al., 2018, Wang et al., 2017a). The V2 null TYLCV mutant was generated with the QuickChange Lightning Site-Directed Mutagenesis Kit (Agilent Technologies, Cat #210518) using the WT infectious clone as template. For the plasmids used for biomolecular fluorescence complementation (BiFC), *NbAGO4*, *SlAGO4,* V2/$V2_{L76S}$ were cloned into entry vector pDONR221-P1P4/pDONR221-P3P2 (Invitrogen) and then Gateway-cloned into the pBiFC-2in1-CN vector (Grefen & Blatt, 2012) as shown in Supplementary table 2. The binary plasmids for split-luciferase complementation imaging assay were generated by Gateway cloning the *NbAGO4, SlAGO4, SlWRKY75* or V2 from pENTR-D/TOPO entry vector into pGWB-N-luc and pGWB-C-luc (Yu et al., 2019). To generate pCAMBIA1300-3xFLAG-NbAGO4-1, pCAMBIA1300 was digested with *Xba*I and *Xma*I, and then the 3xFLAG and NbAGO4-1 coding sequences were amplified by PCR and Infusion-cloned into pCAMBIA1300 with ClonExpress® MultiS One Step Cloning Kit (Vazyme). pDONR207-*Fibrillarin* (Kim et al., 2007b) was used to Gateway-clone *Fibrillarin* to pGWB545 (Nakagawa et al., 2007). All primers and plasmids used for cloning are summarized in Supplementary tables 1 and 2, respectively.

Plant materials and growth conditions

N. benthamiana and tomato plants (cv. Money maker) were grown in a controlled growth chamber under long day conditions (LD, 16 h light/8 h dark) at 25℃.

Agrobacterium-mediated transient gene expression in *N. benthamiana*

All binary plasmids were transformed into *Agrobacterium tumefaciens* strain GV3101, with the exception of pBINTRA6, which was transformed into *A. tumefaciens* strain C58c1. *A. tumefaciens* clones carrying the constructs of interest were liquid-cultured in LB with appropriate antibiotics at 28℃ overnight. Bacterial cultures were then centrifuged at 4,000 g for 10 min and resuspended in the infiltration buffer (10 mM $MgCl_2$, 10 mM MES pH 5.6, 150 μM acetosyringone) and adjusted to an OD_{600} = 0.5. Next, the bacterial suspensions were incubated in the buffer at room temperature and in the dark for 2-4 hours and then infiltrated 3-4-week-old *N. benthamiana* plants. For co-expression experiments, the different agrobacterium suspensions were mixed at 1:1 ratio before infiltration.

Protein extraction and immunoprecipitation assays

Protein extraction and co-immunoprecipitation assays were performed as described in Wang et al., 2017a. Protein extracts were immunoprecipitated with GFP-Trap beads (Chromotek, Germany), and analyzed by western blot with anti-GFP (Abiocode, M0802-3a) and anti-HA (12CA5) (Roche, Cat. No. 11 583 816 001) antibodies.

For 3xFLAG-NbAGO4 IP followed by vsiRNA extraction, 6 grams of *N. benthamiana* leaves transiently expressing 3xFLAG-NbAGO4 were collected, ground in liquid nitrogen and homogenized in 6x (w:v) extraction buffer (20mM Tris HCl pH7.5, 25mM $MgCl_2$, 300mM NaCl, 5mM DTT, 0.5% NP-40, 1x complete™ Protease Inhibitor Cocktail (Roche)) at 4°C with rotation for 30 minutes. The extract was subjected to centrifugation (14,000 rpm, 25min) at 4°C. 5 μg anti-FLAG antibody (Sigma, F3165) per gram of tissue were added to the supernatant in a new tube and incubated at 4°C overnight. The next day, 20 μl of slurry Protein G beads (Invitrogen) per gram of tissue were added and subjected to a further incubation for 2 hours with rotation at 4°C. After incubation, Protein G beads were washed three times in 3x (v:v) homogenate wash buffer (20mM Tris pH7.5, 25mM $MgCl_2$, 300mM NaCl, 0.5% NP-40). The quality of purification was examined by SDS-PAGE followed by immunoblotting.

Split-luciferase complementation imaging assay

Split-luciferase complementation imaging assays were performed as described (Chen et al., 2008). Equal volumes of *A. tumefaciens* harboring V2-N-luc or C-luc-NbAGO4-1/2, C-luc-SlAGO4a/b, or C-luc-SlWRKY75 at OD_{600}=0.5 were mixed at 1:1 ratio. Three different combinations of *A. tumefaciens* were infiltrated on the same *N. benthamiana* leaf. 1mM luciferin

(in H_2O) was infiltrated into the inoculated leaves 2 days after agrobacterium infiltration. A low-light cooled CCD imaging apparatus (NightShade LB985 with IndiGO software) was used to capture and analyse the luciferase signal at 2 dpi.

Confocal imaging

Confocal imaging for co-localization of V2-GFP, RFP-AGO4, and CFP-Fibrillarin upon transient expression in *N. benthamiana* epidermal cells was performed on a Leica TCS SP8 point scanning confocal microscope using the pre-set sequential scan settings for GFP (Ex:488 nm, Em:500–550 nm), RFP (Ex:561 nm, Em:600–650 nm), and CFP (Ex:442 nm, Em:452–482 nm).

Bimolecular Fluorescence Complementation

For bimolecular fluorescence complementation (BiFC) analyses, *A. tumefaciens* clones carrying pBiFC-2in1-CN binary constructs (Grefen and Blat, 2012) and CFP-Fibrillarin were mixed at 1:1 ratio and infiltrated on 3-4-week-old *N. benthamiana* plants. Imaging was performed 2 days later under a Leica TCS SP8 confocal microscope by using the pre-set sequential scan settings for YFP (Ex: 514 nm, Em: 525–575 nm) and for CFP (Ex:442 nm, Em:452–500 nm).

Virus-induced gene silencing

The vectors used for virus-induced gene silencing (VIGS) were pBINTRA6 (Ratcliff et al., 2001) and pTRV2-GW (Taylor et al., 2012). A 362-bp fragment of *NbAGO4-1* cDNA (from nt 1920 to 2281) was amplified using primers shown in Supplementary table 1, cloned into pENTR/D-TOPO (Invitrogen), and subcloned into pTRV2-GW through an LR reaction (Invitrogen) to yield TRV-*NbAGO4*. VIGS assays were performed as described in Lozano-Duran et al., 2011. For TYLCV local infection assays, *A. tumefaciens* carrying pBINTRA6 and TRV-*NbAGO4* or TRV-EV were mixed and inoculated into 18-day-old *N. benthamiana* plants. Two weeks later, fully expanded young leaves were infiltrated with *A. tumefaciens* carrying the TYLCV infectious clone and samples were collected at 3, 4 or 9 days post-inoculation (dpi) to detect viral accumulation. For TYLCV systemic infection assays, *A. tumefaciens* carrying pBINTRA6 and TRV-*NbAGO4* or TRV-EV (empty vector) and the TYLCV infectious clone were mixed and inoculated on 18-day-old *N. benthamiana* plants. The three most apical leaves of each plant were collected at 3 weeks post-inoculation (wpi) to detect viral accumulation.

Quantitative PCR (qPCR) and Reverse Transcription PCR (RT-qPCR)

To determine viral accumulation, total DNA was extracted from *N. benthamiana* leaves (from infiltrated leaves in local infection assays and from apical leaves in systemic infection assays)

using the CTAB method (Minas et al., 2011). Quantitative PCR (qPCR) was performed with primers to amplify Rep (Wang et al., 2017b). As internal reference for DNA detection, the 25S ribosomal DNA interspacer (ITS) was used (Mason et al., 2008). To detect *NbAGO4-1*, *NbAGO4-2*, and *NbAGO6* transcripts, total RNA was extracted from *N. benthamiana* leaves by using Plant RNA kit (OMEGA Bio-tek # R6827). RNA was reverse-transcribed into cDNA by using the iScriptTM cDNA Synthesis Kit (Bio-Rad #1708890) according to the manufacturer's instructions. *NbTubulin* was used as reference gene (Liu et al., 2012). Relative expression was calculated by the comparative Ct method (2-ΔΔCt). qPCR and RT-qPCR were performed in a BioRad CFX96 real-time system as described previously (Wang et al., 2017b). Total RNA was extracted from the leaves of tomato plants mock-inoculated or infected with TYLCV at 3 weeks post-inoculation (wpi). *SlActin was used as* reference gene (Exposito-Rodriguez et al., 2008). Similarly, RT-qPCR was performed on RNA extracted from tomato to detect the expression of *SlAGO4a/d/c/d*. All primers used for qPCR and qRT-PCR are listed in Supplementary Table 3.

DNA bisulfite sequencing analysis

DNA from virus-infected plant tissues was extracted by Dneasy Plant Mini Kit (QIAGEN, Cat. No. 69104), and 500 ng of purified DNA was subjected to bisulfite treatment using EpiTect Plus DNA Bisulfite Kit (QIAGEN, Cat. No. 59124) according to the manufacturer's handbook. The selected fragment (viral IR) of the bisulfite-treated DNA was amplified by PCR (Fw: TTTGATGTATTTTTTATTTGTTGGGGTTT, Rv: CCCTTACAACARATATAARATCCCT); amplified fragments were cloned into the pMD18-T vector by TA ligation and sequenced (>15 clones per experiment). Cytosine methylation analysis was performed with Kismeth (http://katahdin.mssm.edu/kismeth/revpage.pl) (Gruntman et al., 2008).

Chromatin immunoprecipitation (ChIP) assay

The agrobacterium clone carrying the binary vector to express 3xFLAG-NbAGO4-1 was co-infiltrated with those carrying the TYLCV or TYLCV-V2null infectious clones in *N. benthamiana* leaves, and tissues were collected at 2 dpi. Chromatin immunoprecipitation (ChIP) assays were performed as described (He et al., 2018). In brief, the cross-linking of 2 grams of leaves was performed with 1% formaldehyde in 1xPBS buffer and stopped with 1/15 volume of 2 M glycine by vacuum infiltration. Then the tissue was ground to powder and resuspended in HB buffer (2.5% Ficoll 400, 5% Dextran T40, 0.4 M Sucrose, 25 mM Tris pH 7.4, 10 mM MgCl2, 0.035% β-mercaptoethanol, 1% Protease Inhibitor Cocktail (Sigma)), homogenized and filtered through Miracloth (Milli-pore). Triton x-100 was added to the supernatant until final concentration was

0.5%. After spinning at 2,000×g for 20 min at 4°C, the pellet was re-suspended in HB buffer containing 0.1% Triton x-100 and spun at 2,000×g for 10 min at 4°C. Isolated nuclei were re-suspended in 500 µl of Nuclei Lysis buffer and sonicated by BioruptorTM UCD-200 sonicator (diagenode) for 30 min. Following centrifugation at 21,130×g for 5 min at 4°C, the supernatant was separated and used for input and immunoprecipitation. After adding 9 volume of ChIP dilution buffer to the supernatant, this was pre-cleared with 10 µl of Dynabeads Protein G (Invirogen) for 1 h at 4°C. After removing the beads from the mixture, the supernatant was incubated with anti-FLAG antibody (Sigma, F3165), or anti-IgG antibody (Sigma, I5006) overnight at 4°C. The following day, after adding 20 µl of Dynabeads Protein G, the mixture was incubated for 2 h at 4°C. Beads were sequentially washed with 1 ml of the following buffers: Low Salt Wash buffer (150 mM NaCl, 0.1% SDS, 1% Triton x-100, 2 mM EDTA, 20 mM Tris pH 8.0), High Salt Wash buffer (500 mM NaCl, 0.1% SDS, 1% Triton x-100, 2 mM EDTA, 20 mM Tris pH 8.0), LiCl wash buffer (250 mM LiCl, 1% Igepal, 1% Sodium Deoxycholate, 1 mM EDTA, 10 mM Tris pH 8.0), TE buffer (10 mM Tris pH 8.0, 1 mM EDTA). Immunocomplexes were eluted with 250 µl of Elution buffer (1% SDS, 0.1 M $NaHCO_3$) at 65°C for 15 min. After reverse crosslinking, 10 µl of 0.5 M EDTA, 20 µl of 1 M Tris pH 6.5 and 1 µl of proteinase K (Invitrogen) were added to each sample, which was incubated at 45 °C for 2 h. DNA was then purified using QIAquick PCR Purification Kit (QIAGEN, Cat. No. 28106). The products were eluted into 200 µl of ddH_2O, and analysed by qPCR. The primers used in this experiment are listed in Supplementary Table 3; the primers for *Actin* are taken from Maimbo et al., 2010.

Small RNA (sRNA) extraction and northern blot analysis

Small RNA (sRNA) extraction and northern blot was performed as described (Yang et al., 2015). Briefly, sRNAs were purified from total extracts or AGO4 immunoprecipitates and subjected to northern blot analysis. For each sample, sRNAs were separated on a 17% polyacrylamide gel, which was electrotransferred to a Hybond N+ membrane (GE Lifesciences). Membranes were cross-linked, incubated for 2 hours at 65°C, and hybridized overnight at 38°C with ^{32}P-labeled probes for the intergenic region (IR) of the viral genome amplified by PCR (Fw: TCCTCTTTAGAGAGAGAACAATTGGGA, Rv: ACAACGAAATCCGTGAACAG) or oligonucleotides in PerfectHyb buffer (Sigma). Washed membranes were exposed to X-ray films at −80 °C for 3 days.

ACKNOWLEDGEMENTS

The authors thank Xinyu Jian, Aurora Luque, and Yujing (Ada) Liu for technical assistance, Gang Yu and Alberto Macho for sharing materials, and all members in Rosa Lozano-Duran's and Alberto Macho's groups for stimulating discussions and helpful suggestions. The authors are grateful to Alberto Macho, Huang Tan, and Tamara Jimenez-Gongora for critical reading of the manuscript. This research was supported by the Strategic Priority Research Program of the Chinese Academy of Sciences (Grant No. XDB27040206), and by the National Natural Science Foundation of China (NSFC) (grant numbers 31671994 and 31870250). Research in RL-D's lab is funded by the Shanghai Center for Plant Stress Biology of the Chinese Academy of Sciences and the 100 Talent Program of the Chinese Academy of Sciences.

AUTHOR CONTRIBUTIONS

RL-D and LW conceived the project; LW, DY, LH, and GZ performed experiments and analyzed results; all authors intellectually contributed to the project; RL-D wrote the manuscript, with input from all authors.

CONFLICT OF INTEREST

The authors declare no conflict of interest.

REFERENCES

Böhmdorfer G, Rowley MJ, Kuciński J, Zhu Y, Amies I, Wierzbicki AT (2014) RNA-directed DNA methylation requires stepwise binding of silencing factors to long non-coding RNA. *The Plant Journal* 79: 181-191

Bai M, Yang GS, Chen WT, Mao ZC, Kang HX, Chen GH, Yang YH, Xie BY (2012) Genome-wide identification of Dicer-like, Argonaute and RNA-dependent RNA polymerase gene families and their expression analyses in response to viral infection and abiotic stresses in Solanum lycopersicum. *Gene* 501: 52-62

Barneche F, Steinmetz F, Echeverria M (2000) Fibrillarin genes encode both a conserved nucleolar protein and a novel small nucleolar RNA involved in ribosomal RNA methylation in Arabidopsis thaliana. *The Journal of biological chemistry* 275: 27212-20

Brosseau C, El Oirdi M, Adurogbangba A, Ma X, Moffett P (2016) Antiviral Defense Involves AGO4 in an Arabidopsis-Potexvirus Interaction. *Molecular plant-microbe interactions : MPMI* 29: 878-888

Brough CL, Gardiner WE, Inamdar NM, Zhang XY, Ehrlich M, Bisaro DM (1992) DNA methylation inhibits propagation of tomato golden mosaic virus DNA in transfected protoplasts. *Plant Mol Biol* 18: 703-12

Buchmann RC, Asad S, Wolf JN, Mohannath G, Bisaro DM (2009) Geminivirus AL2 and L2 proteins suppress transcriptional gene silencing and cause genome-wide reductions in cytosine methylation. *Journal of virology* 83: 5005-13

Burgyán J, Havelda Z (2011) Viral suppressors of RNA silencing. *Trends Plant Science* 16(5):265-72.

Butterbach P, Verlaan MG, Dullemans A, Lohuis D, Visser RG, Bai Y, Kormelink R (2014) Tomato yellow leaf curl virus resistance by Ty-1 involves increased cytosine methylation of viral genomes and is compromised by cucumber mosaic virus infection. *Proceedings of the National Academy of Sciences of the United States of America* 111: 12942-7

Castillo-Gonzalez C, Liu X, Huang C, Zhao C, Ma Z, Hu T, Sun F, Zhou Y, Zhou X, Wang XJ, Zhang X (2015) Geminivirus-encoded TrAP suppressor inhibits the histone methyltransferase SUVH4/KYP to counter host defense. *eLife* 4

Ceniceros-Ojeda EA, Rodriguez-Negrete EA, Rivera-Bustamante RF (2016) Two Populations of Viral Minichromosomes Are Present in a Geminivirus-Infected Plant Showing Symptom Remission (Recovery). *Journal of virology* 90: 3828-3838

Chan SW, Henderson IR, Jacobsen SE (2005) Gardening the genome: DNA methylation in Arabidopsis thaliana. *Nature reviews Genetics* 6: 351-60

Chen H, Zou Y, Shang Y, Lin H, Wang Y, Cai R, Tang X, Zhou JM (2008) Firefly luciferase complementation imaging assay for protein-protein interactions in plants. *Plant physiology* 146: 368-76

Coursey T, Regedanz E, Bisaro DM (2018) Arabidopsis RNA Polymerase V Mediates Enhanced Compaction and Silencing of Geminivirus and Transposon Chromatin during Host Recovery from Infection. 92

Dereeper A, Audic S, Claverie JM, Blanc G (2010) BLAST-EXPLORER helps you building datasets for phylogenetic analysis. *BMC evolutionary biology* 10: 8

Dereeper A, Guignon V, Blanc G, Audic S, Buffet S, Chevenet F, Dufayard JF, Guindon S, Lefort V, Lescot M, Claverie JM, Gascuel O (2008) Phylogeny.fr: robust phylogenetic analysis for the non-specialist. *Nucleic acids research* 36: W465-9

Deuschle K, Kepp G, Jeske H (2016) Differential methylation of the circular DNA in geminiviral minichromosomes. *Virology* 499: 243-258

Dogar AM (2006) RNAi dependent epigenetic marks on a geminivirus promoter. *Virology journal* 3: 5

Ermak G, Paszkowski U, Wohlmuth M, Mittelsten Scheid O, Paszkowski J (1993) Cytosine methylation inhibits replication of African cassava mosaic virus by two distinct mechanisms. *Nucleic acids research* 21: 3445-50

Exposito-Rodriguez M, Borges AA, Borges-Perez A, Perez JA (2008) Selection of internal control genes for quantitative real-time RT-PCR studies during tomato development process. *BMC plant biology* 8: 131

Gao Z, Liu H-L, Daxinger L, Pontes O, He X, Qian W, Lin H, Xie M, Lorkovic ZJ, Zhang S (2010) An RNA polymerase II-and AGO4-associated protein acts in RNA-directed DNA methylation. *Nature* 465: 106

Grefen C, Blatt MR (2012) A 2in1 cloning system enables ratiometric bimolecular fluorescence complementation (rBiFC). *BioTechniques* 53: 311-14

Gruntman E, Qi Y, Slotkin RK, Roeder T, Martienssen RA, Sachidanandam R (2008) Kismeth: analyzer of plant methylation states through bisulfite sequencing. *BMC bioinformatics* 9: 371

Haag JR, Ream TS, Marasco M, Nicora CD, Norbeck AD, Pasa-Tolic L, Pikaard CS (2012) In vitro transcription activities of Pol IV, Pol V, and RDR2 reveal coupling of Pol IV and RDR2 for dsRNA synthesis in plant RNA silencing. *Molecular cell* 48: 811-818

Hanley-Bowdoin L, Bejarano ER, Robertson D, Mansoor S (2013) Geminiviruses: masters at redirecting and reprogramming plant processes. *Nature reviews Microbiology* 11: 777-88

He L, Wu W, Zinta G, Yang L, Wang D, Liu R, Zhang H, Zheng Z, Huang H, Zhang Q, Zhu J-K (2018) A naturally occurring epiallele associates with leaf senescence and local climate adaptation in Arabidopsis accessions. *Nature communications* 9: 460

Ismayil A, Haxim Y, Wang Y, Li H, Qian L, Han T, Chen T, Jia Q, Yihao Liu A, Zhu S, Deng H, Gorovits R, Hong Y, Hanley-Bowdoin L, Liu Y (2018) Cotton Leaf Curl Multan virus C4 protein suppresses both transcriptional and post-transcriptional gene silencing by interacting with SAM synthetase. *PLoS pathogens* 14: e1007282

533 Jackel JN, Storer JM, Coursey T, Bisaro DM (2016) Arabidopsis RNA Polymerases IV and V Are
534 Required To Establish H3K9 Methylation, but Not Cytosine Methylation, on Geminivirus
535 Chromatin. *Journal of virology* 90: 7529-40
536
537 Kim SH, Macfarlane S, Kalinina NO, Rakitina DV, Ryabov EV, Gillespie T, Haupt S, Brown JW,
538 Taliansky M (2007a) Interaction of a plant virus-encoded protein with the major nucleolar protein
539 fibrillarin is required for systemic virus infection. *Proceedings of the National Academy of Sciences*
540 *of the United States of America* 104: 11115-20
541
542 Kim SH, Ryabov EV, Kalinina NO, Rakitina DV, Gillespie T, MacFarlane S, Haupt S, Brown JW,
543 Taliansky M (2007b) Cajal bodies and the nucleolus are required for a plant virus systemic
544 infection. *The EMBO journal* 26: 2169-79
545
546 Kushwaha NK, Mansi, Chakraborty S (2017) The replication initiator protein of a geminivirus
547 interacts with host monoubiquitination machinery and stimulates transcription of the viral genome.
548 *PLoS pathogens* 13: e1006587
549
550 Law JA, Vashisht AA, Wohlschlegel JA, Jacobsen SE (2011) SHH1, a homeodomain protein
551 required for DNA methylation, as well as RDR2, RDM4, and chromatin remodeling factors,
552 associate with RNA polymerase IV. *PLoS genetics* 7: e1002195
553
554 Li CF, Henderson IR, Song L, Fedoroff N, Lagrange T, Jacobsen SE (2008) Dynamic regulation
555 of ARGONAUTE4 within multiple nuclear bodies in Arabidopsis thaliana. *PLoS genetics* 4: e27
556
557 Li CF, Pontes O, El-Shami M, Henderson IR, Bernatavichute YV, Chan SW, Lagrange T, Pikaard
558 CS, Jacobsen SE (2006) An ARGONAUTE4-containing nuclear processing center colocalized
559 with Cajal bodies in Arabidopsis thaliana. *Cell* 126: 93-106
560
561 Liu D, Shi L, Han C, Yu J, Li D, Zhang Y (2012) Validation of reference genes for gene expression
562 studies in virus-infected Nicotiana benthamiana using quantitative real-time PCR. *PloS one* 7:
563 e46451
564
565 Lozano-Duran R, Rosas-Diaz T, Luna AP, Bejarano ER (2011) Identification of host genes
566 involved in geminivirus infection using a reverse genetics approach. *PloS one* 6: e22383

Ma X, Nicole MC, Meteignier LV, Hong N, Wang G, Moffett P (2015) Different roles for RNA silencing and RNA processing components in virus recovery and virus-induced gene silencing in plants. *Journal of experimental botany* 66: 919-32

Maimbo M, Ohnishi K, Hikichi Y, Yoshioka H, Kiba A (2010) S-glycoprotein-like protein regulates defense responses in Nicotiana plants against Ralstonia solanacearum. *Plant physiology* 152: 2023-35

Mason G, Caciagli P, Accotto GP, Noris E (2008) Real-time PCR for the quantitation of Tomato yellow leaf curl Sardinia virus in tomato plants and in Bemisia tabaci. *Journal of virological methods* 147: 282-9

Matzke MA, Kanno T, Matzke AJ (2015) RNA-Directed DNA Methylation: The Evolution of a Complex Epigenetic Pathway in Flowering Plants. *Annual review of plant biology* 66: 243-67

Matzke MA, Mosher RA (2014) RNA-directed DNA methylation: an epigenetic pathway of increasing complexity. *Nature reviews Genetics* 15: 394-408

Minas K, McEwan NR, Newbold CJ, Scott KP (2011) Optimization of a high-throughput CTAB-based protocol for the extraction of qPCR-grade DNA from rumen fluid, plant and bacterial pure cultures. *FEMS microbiology letters* 325: 162-9

Minoia S, Carbonell A, Di Serio F, Gisel A, Carrington JC, Navarro B, Flores R (2014) Specific argonautes selectively bind small RNAs derived from potato spindle tuber viroid and attenuate viroid accumulation in vivo. *Journal of virology* 88: 11933-45

Nakagawa T, Suzuki T, Murata S, Nakamura S, Hino T, Maeo K, Tabata R, Kawai T, Tanaka K, Niwa Y, Watanabe Y, Nakamura K, Kimura T, Ishiguro S (2007) Improved Gateway binary vectors: high-performance vectors for creation of fusion constructs in transgenic analysis of plants. *Bioscience, biotechnology, and biochemistry* 71: 2095-100

Piedra-Aguilera A, Jiao C, Luna AP, Villanueva F, Dabad M, Esteve-Codina A, Diaz-Pendon JA, Fei Z, Bejarano ER, Castillo AG (2019) Integrated single-base resolution maps of transcriptome,

601 sRNAome and methylome of Tomato yellow leaf curl virus (TYLCV) in tomato. *Scientific reports*
602 9: 2863
603
604 Raja P, Sanville BC, Buchmann RC, Bisaro DM (2008) Viral genome methylation as an epigenetic
605 defense against geminiviruses. *Journal of virology* 82: 8997-9007
606
607 Ratcliff F, Martin-Hernandez AM, Baulcombe DC (2001) Technical Advance. Tobacco rattle virus
608 as a vector for analysis of gene function by silencing. *The Plant journal : for cell and molecular*
609 *biology* 25: 237-45
610
611 Rawlings RA, Krishnan V, Walter NG (2011) Viral RNAi suppressor reversibly binds siRNA to
612 outcompete Dicer and RISC via multiple turnover. *Journal of Molecular Biology* 408(2):262-76.
613
614 Rodriguez-Negrete E, Lozano-Duran R, Piedra-Aguilera A, Cruzado L, Bejarano ER, Castillo AG
615 (2013) Geminivirus Rep protein interferes with the plant DNA methylation machinery and
616 suppresses transcriptional gene silencing. *The New phytologist* 199: 464-75
617
618 Rosas-Diaz T, Zhang D, Fan P, Wang L, Ding X, Jiang Y, Jimenez-Gongora T, Medina-Puche L,
619 Zhao X, Feng Z, Zhang G, Liu X, Bejarano ER, Tan L, Zhang H, Zhu JK, Xing W, Faulkner C,
620 Nagawa S, Lozano-Duran R (2018) A virus-targeted plant receptor-like kinase promotes cell-to-
621 cell spread of RNAi. *Proceedings of the National Academy of Sciences of the United States of*
622 *America* 115: 1388-1393
623
624 Schott G, Mari-Ordonez A, Himber C, Alioua A, Voinnet O, Dunoyer P (2012) Differential effects
625 of viral silencing suppressors on siRNA and miRNA loading support the existence of two distinct
626 cellular pools of ARGONAUTE1. *The EMBO journal* 31: 2553-65
627
628 Semashko MA, Rakitina DV, Gonzalez I, Canto T, Kalinina NO, Taliansky ME (2012) Movement
629 protein of hordeivirus interacts in vitro and in vivo with coilin, a major structural protein of Cajal
630 bodies. *Doklady Biochemistry and biophysics* 442: 57-60
631
632 Shaw J, Love AJ, Makarova SS, Kalinina NO, Harrison BD, Taliansky ME (2014) Coilin, the
633 signature protein of Cajal bodies, differentially modulates the interactions of plants with viruses in
634 widely different taxa. *Nucleus* 5: 85-94

Taylor KW, Kim JG, Su XB, Aakre CD, Roden JA, Adams CM, Mudgett MB (2012) Tomato TFT1 is required for PAMP-triggered immunity and mutations that prevent T3S effector XopN from binding to TFT1 attenuate Xanthomonas virulence. *PLoS pathogens* 8: e1002768

Torchetti EM, Pegoraro M, Navarro B, Catoni M, Di Serio F, Noris E (2016) A nuclear-replicating viroid antagonizes infectivity and accumulation of a geminivirus by upregulating methylation-related genes and inducing hypermethylation of viral DNA. *Scientific reports* 6: 35101

Tu YC, Tsai WS, Wei JY, Chang KY, Tien CC, Hsiao HY, Fu SF (2017) The C2 protein of tomato leaf curl Taiwan virus is a pathogenicity determinant that interferes with expression of host genes encoding chromomethylases. *Physiologia plantarum* 161: 515-531

Wang B, Li F, Huang C, Yang X, Qian Y, Xie Y, Zhou X (2014) V2 of tomato yellow leaf curl virus can suppress methylation-mediated transcriptional gene silencing in plants. *The Journal of general virology* 95: 225-30

Wang B, Yang X, Wang Y, Xie Y, Zhou X (2018) Tomato Yellow Leaf Curl Virus V2 Interacts with Host Histone Deacetylase 6 To Suppress Methylation-Mediated Transcriptional Gene Silencing in Plants. *Journal of virology* 92

Wang L, Ding X, Xiao J, Jimenez-Gomicronngora T, Liu R, Lozano-Duran R (2017a) Inference of a Geminivirus-Host Protein-Protein Interaction Network through Affinity Purification and Mass Spectrometry Analysis. *Viruses* 9

Wang L, Tan H, Wu M, Jimenez-Gongora T, Tan L, Lozano-Duran R (2017b) Dynamic Virus-Dependent Subnuclear Localization of the Capsid Protein from a Geminivirus. *Frontiers in plant science* 8: 2165

Wang Y, Wu Y, Gong Q, Ismayil A, Yuan Y, Lian B, Jia Q, Han M, Deng H, Hong Y, Hanley-Bowdoin L, Qi Y, Liu Y (2019) Geminiviral V2 Protein Suppresses Transcriptional Gene Silencing through Interaction with AGO4. *Journal of virology* 93

668 Wartig L, Kheyr-Pour A, Noris E, De Kouchkovsky F, Jouanneau F, Gronenborn B, Jupin I (1997)
669 Genetic analysis of the monopartite tomato yellow leaf curl geminivirus: roles of V1, V2, and C2
670 ORFs in viral pathogenesis. *Virology* 228: 132-40
671
672 Woo HR, Dittmer TA, Richards EJ (2008) Three SRA-domain methylcytosine-binding proteins
673 cooperate to maintain global CpG methylation and epigenetic silencing in Arabidopsis. *PLoS*
674 *genetics* 4: e1000156
675
676 Xie Z, Johansen LK, Gustafson AM, Kasschau KD, Lellis AD, Zilberman D, Jacobsen SE,
677 Carrington JC (2004) Genetic and functional diversification of small RNA pathways in plants.
678 *PLoS biology* 2: e104
679
680 Yadav RK, Chattopadhyay D (2011) Enhanced viral intergenic region-specific short interfering
681 RNA accumulation and DNA methylation correlates with resistance against a geminivirus.
682 *Molecular plant-microbe interactions : MPMI* 24: 1189-97
683
684 Yang D-L, Zhang G, Tang K, Li J, Yang L, Huang H, Zhang H, Zhu J-K (2015) Dicer-independent
685 RNA-directed DNA methylation in Arabidopsis. *Cell research*
686
687 Yang LP, Fang YY, An CP, Dong L, Zhang ZH, Chen H, Xie Q, Guo HS (2013) C2-mediated
688 decrease in DNA methylation, accumulation of siRNAs, and increase in expression for genes
689 involved in defense pathways in plants infected with beet severe curly top virus. *The Plant journal :*
690 *for cell and molecular biology* 73: 910-7
691
692 Yang X, Xie Y, Raja P, Li S, Wolf JN, Shen Q, Bisaro DM, Zhou X (2011) Suppression of
693 methylation-mediated transcriptional gene silencing by betaC1-SAHH protein interaction during
694 geminivirus-betasatellite infection. *PLoS pathogens* 7: e1002329
695
696 Yu G, Xian L, Xue H, Yu W, Rufian J, Sang Y, Morcillo R, Wang Y, Macho AP (2019) A bacterial
697 effector protein prevents MAPK-mediated phosphorylation of SGT1 to suppress plant immunity.
698 *bioRxiv*: 641241
699 Zhang Z, Chen H, Huang X, Xia R, Zhao Q, Lai J, Teng K, Li Y, Liang L, Du Q, Zhou X, Guo H,
700 Xie Q (2011) BSCTV C2 attenuates the degradation of SAMDC1 to suppress DNA methylation-
701 mediated gene silencing in Arabidopsis. *The Plant cell* 23: 273-88

Zhong X, Du J, Hale CJ, Gallego-Bartolome J, Feng S, Vashisht AA, Chory J, Wohlschlegel JA, Patel DJ, Jacobsen SE (2014) Molecular mechanism of action of plant DRM de novo DNA methyltransferases. *Cell* 157: 1050-1060

Zhong X, Wang ZQ, Xiao R, Wang Y, Xie Y, Zhou X (2017) iTRAQ analysis of the tobacco leaf proteome reveals that RNA-directed DNA methylation (RdDM) has important roles in defense against geminivirus-betasatellite infection. *Journal of proteomics* 152: 88-101

Zilberman D, Cao X, Jacobsen SE (2003) ARGONAUTE4 control of locus-specific siRNA accumulation and DNA and histone methylation. *Science (New York, NY)* 299: 716-719

FIGURE LEGENDS

Figure 1. V2 interacts with AGO4 from *N. benthamiana*.

A Unique peptide count, protein coverage, and best Mascot Score of NbAGO4-1 and NbAGO4-2 co-immunoprecipitated with V2-GFP, as identified by affinity purification followed by mass spectrometry (AP-MS). Results from three independent biological repeats are shown. "-" indicates no peptide was detected.

B 3xHA-NbAGO4-1 and 3xHA-NbAGO4-2 specifically interact with V2-GFP in co-immunoprecipitation (co-IP) assays upon transient expression in *N. benthamiana*. Free GFP was used as negative control. CBB, Coomassie brilliant blue staining. Three independent biological replicates were performed with similar results.

C NbAGO4-1 and NbAGO4-2 interact with V2 in split-luciferase assays. V2-N-luc and C-luc-NbAGO4-1/2 were transiently co-expressed in *N. benthamiana*; C-luc-SlWRKY75 is used as negative control. The luciferase bioluminescence from at least three independent leaves per experiment was imaged two days after infiltration. The average bioluminescence, measured in counts per second (cps), as well as an image of a representative leaf are shown. Values represent the mean of three independent biological replicates; error bars indicate SEM. Asterisks indicate a statistically significant difference (according to a Student's *t*-test, **: $P<0.01$, ***: $P<0.001$.) compared to the negative control.

Figure 2. V2 interacts with AGO4 from tomato.

A Phylogenetic tree of AtAGO4, NbAGO4, and SlAGO4 proteins. The phylogenetic analysis was performed with phylogeny.fr (Dereeper et al., 2010, Dereeper et al., 2008).

B Pairwise identity and genetic distance matrix among AtAGO4, NbAGO4 and SlAGO4 proteins. The analysis was performed by Geneious (https://www.geneious.com).

C 3xHA-SlAGO4a, 3xHA-SlAGO4b, and 3xHA-SlAGO4d specifically interact with V2-GFP in co-immunoprecipitation (co-IP) assays upon transient expression in *N. benthamiana*. Free GFP was used as negative control. CBB, Coomassie brilliant blue staining. Three independent biological replicates were performed with similar results.

D SlAGO4a and SlAGO4b interact with V2 in split-luciferase assays. V2-N-luc and C-luc-SlAGO4a/b were transiently co-expressed in *N. benthamiana*; C-luc-SlWRKY75 is used as

745 negative control. The luciferase bioluminescence from at least three independent leaves per
746 experiment was imaged two days after infiltration. The average bioluminescence, measured
747 in counts per second (cps), as well as an image of a representative leaf are shown. Values
748 represent the mean of three independent biological replicates; error bars indicate SEM.
749 Asterisks indicate a statistically significant difference (according to a Student's *t*-test, ***:
750 P<0.001.) compared to the negative control.

751

752 **Figure 3. V2 interacts with AGO4 in the Cajal body.**

753 A V2-GFP and RFP-AGO4 co-localize in the Cajal body. CFP-Fibrillarin, V2-GFP and RFP-
754 NbAGO4-1/2 or RFP-SlAGO4a/b/d were transiently co-expressed in *N. benthamiana*
755 epidermal cells. CFP-Fibrillarin is used as a nucleolus and Cajal body marker. Confocal
756 images were taken at two days after infiltration . Arrowheads indicate the position of the Cajal
757 body. Bar, 5µm. This experiment was repeated more than three times with similar results.

758 B V2 interacts with AGO4 in the Cajal body. The N-terminal half of the YFP fused to V2 (V2-
759 nYFP) was transiently co-expressed with the C-terminal half of the YFP alone (cYFP, as a
760 negative control), or cYFP-NbAGO4, cYFP-SlAGO4, or cYFP-V2 (as a positive control) in *N.*
761 *benthamiana* leaves. CFP-Fibrillarin was used as a nucleolus and Cajal body marker.
762 Confocal images were taken at two days after infiltration. Yellow fluorescence indicates a
763 positive interaction. Arrowheads indicate the position of the Cajal body. Bar, 5µm. This
764 experiment was repeated more than three times with similar results.

765

766 **Figure 4. V2 counters the AGO4-dependent defence to promote virulence**

767 A Expression of *NbAGO4-1, NbAGO4-2,* and *NbAGO6* in *N. benthamiana* plants infected with
768 TRV-EV (empty vector) or TRV-*NbAGO4*, measured by reverse transcription quantitative real-
769 time PCR (RT-qPCR). Gene expression was normalized to *NbTubulin*. Values are the mean
770 of four independent biological replicates; error bars indicate SEM. Asterisks indicate a
771 statistically significant difference according to Student's *t*-test. **: P<0.01, ***: P<0.001, ns:
772 not significant.

773 B Representative pictures of *N. benthamiana* plants infected with the indicated combinations of
774 viruses. Photographs were taken at 3 weeks post-inoculation (wpi).

C *NbAGO4-1* expression in *NbAGO4*-silenced plants and control plants infected with TYLCV, TYLCV-V2null, or mock-inoculated at 3 wpi measured by RT-qPCR. Gene expression was normalized to *NbTubulin*. Values are the mean of six independent biological replicates; error bars indicate SEM. Asterisks indicate a statistically significant difference according to Student's *t*-test. *: P<0.05, **: P<0.01, ****: P<0.0001.

D *NbAGO4-2* expression in *NbAGO4*-silenced plants and control plants infected by TYLCV, TYLCV-V2null or mock-inoculated at 3 wpi measured by RT-qPCR. Gene expression was normalized to *Tubulin*. Values are the mean of six independent biological replicates; error bars indicate SEM. Asterisks indicate a statistically significant difference according to Student's *t*-test. *: P<0.05, **: P<0.01, ***: P<0.001.

E Viral (TYLCV) accumulation in local infections in *NbAGO4*-silenced or control plants, measured by qPCR. Infiltrated leaf patches from different plants were collected at 4 dpi. The experimental design is shown in Figure S3A. The accumulation of viral DNA is normalized to the *25S ribosomal RNA interspacer (ITS)*. Values are the mean of eight independent biological replicates; error bars indicate SEM.

F Viral (TYLCV) accumulation in systemic infections in *NbAGO4*-silenced or control plants, measured by qPCR. Apical leaves from six plants were collected at 3 wpi. The experimental design is shown in Figure S3B. The accumulation of viral DNA is normalized to the *25S ribosomal RNA interspacer (ITS)*. Four independent biological replicates were performed with similar results; one representative result is shown. Values are the mean of six independent biological replicates; error bars indicate SEM. Asterisks indicate a statistically significant difference according to Student's *t*-test. *: P<0.05, ***: P<0.001. The relative fold change of viral accumulation between *NbAGO4*-silenced plants and control plants is shown above each column.

Figure 5. V2 suppresses the AGO4-dependent methylation of viral DNA.

A Percentage of methylated cytosines in the intergenic region (IR) of TYLCV in local infection assays with TYLCV WT or V2 null mutant (TYLCV-V2null) in *N. benthamiana* at 3 or 9 days post-inoculation (dpi), as detected by bisulfite sequencing. The original single-base resolution bisulfite sequencing data are shown in Figure S4. Values are the mean of three independent biological replicates; error bars indicate SEM. Asterisks indicate a statistically significant

806 difference according to Student's *t*-test. ***: P<0.001.

807 B Percentage of methylated cytosines in the intergenic region (IR) of TYLCV in local infection
808 assays with the V2 null mutant TYLCV (TYLCV-V2null) in *AGO4*-silenced (TRV-*NbAGO4*) or
809 control (TRV-EV) *N. benthamiana* plants at 4 dpi, as detected by bisulfite sequencing.
810 Samples come from the same plants used in Figure 4E. The original single-base resolution
811 bisulfite sequencing data are shown in Figure S5. Values are the mean of four independent
812 biological replicates; error bars indicate SEM. Asterisks indicate a statistically significant
813 difference according to Student's *t*-test. *: P<0.05.

814 C Percentage of methylated cytosines in the intergenic region (IR) of TYLCV in systemic
815 infection assays with TYLCV WT or V2 null mutant (TYLCV-V2null) in *AGO4*-silenced (TRV-
816 NbAGO4) or control (TRV-EV) *N. benthamiana* plants at 3 weeks post-inoculation (wpi), as
817 detected by bisulfite sequencing. Samples come from the same plants used in Figure 4F.
818 The original single-base resolution bisulfite sequencing data are shown in Figure S6. Values
819 are the mean of four independent biological replicates; error bars indicate SEM. Asterisks
820 indicate a statistically significant difference according to Student's *t*-test. *: P<0.05.

821

822 **Figure 6. V2 interferes with AGO4 binding to the viral genome but does not hamper**
823 **production or loading of vsiRNA.**

824 A 3xFLAG-NbAGO4-1 binds the viral (TYLCV) genome. Binding was detected by chromatin
825 immunoprecipitation (ChIP) upon transient expression in *N. benthamiana* followed by qPCR.
826 Two regions of the viral genome, the IR and the V2 ORF, were analyzed; *ACTIN* was used
827 as negative control. Values represent the mean of four independent biological replicates;
828 error bars represent SEM. Asterisks indicate a significant difference according to a Student's
829 *t*-test; the *P*-value for the different comparisons is shown. *: P<0.05.

830 B NbAGO4-1 binds viral small interfering RNA (vsiRNA) independently of V2. Northern blot of
831 vsiRNA in total extracts or 3xFLAG-NbAGO4 immunoprecipitates (NbAGO4-IP) of *N.*
832 *benthamiana* leaf patches infiltrated with TYLCV WT or V2 null mutant infectious clones
833 (TYLCV, TYLCV-V2null) at two days after infiltration . Detection was performed with a ^{32}P-
834 labeled DNA probe for the intergenic region (IR).

835

836

SUPPLEMENTARY MATERIALS

Supplemental Table S1. List of primers used for cloning in this study.

Supplemental Table S2. List of plasmids used in this study.

Supplemental Table S3. List of primers used for qPCR and qRT-PCR in this study.

SUPPLEMENTARY FIGURE LEGENDS

Figure S1. *SlAGO4* expression in TYLCV-infected and control tomato plants.

SlAGO4a/b/c/d expression in TYLCV-infected or control (mock-inoculated) tomato plants at 3 weeks post-inoculation (wpi), as measured by qRT-PCR. Gene expression was normalized to *SlActin.* Values are the mean of three independent biological replicates; error bars indicate SEM.

Figure S2. V2 is essential for systemic infection in tomato and *N. benthamiana*.

A Design of the V2 null TYLCV mutant used in this work. The second codon of the V2 ORF, originally encoding a Trp (TGG), is mutated to STOP codon (TAG).

B Representative pictures of tomato plants infected with TYLCV WT or V2 null mutant (TYLCV-V2null) or mock-inoculated. Photographs were taken at 3 weeks post-inoculation (wpi). Bar, 5cm.

C Height of tomato plants infected with TYLCV WT or V2 null mutant (TYLCV-V2null) or mock-inoculated at 3 wpi. Values are the mean of five independent biological replicates; error bars indicate SEM.

D Viral (TYLCV) accumulation in tomato plants infected with TYLCV WT or V2 null mutant (TYLCV-V2null) or mock-inoculated at 3 wpi, measured by qPCR. Each sample corresponds to the apical leaves from six plants. The accumulation of viral DNA is normalized to the *25S ribosomal RNA interspacer* (*ITS*). Values are the mean of six independent biological replicates; error bars indicate SEM.

E Representative pictures of *N. benthamiana* plants infected with TYLCV WT or V2 null mutant (TYLCV-V2null) or mock-inoculated. Photographs were taken at 3 weeks post-inoculation (wpi). Bar, 5cm.

F Viral (TYLCV) accumulation in *N. benthamiana* plants infected with TYLCV WT or V2 null mutant (TYLCV-V2null) or mock-inoculated at 3 wpi, measured by qPCR. Each sample corresponds to the apical leaves from six plants. The accumulation of viral DNA is normalized to the *25S ribosomal RNA interspacer (ITS)*. Values are the mean of six independent biological replicates; error bars indicate SEM.

Figure S3. Experimental design for local and systemic TYLCV infection assays in *NbAGO4*-silenced *N. benthamiana* plants.

A Experimental design for local TYLCV infection assays. *A. tumefaciens* carrying the TRV-EV or TRV-*NbAGO4* infectious clones were inoculated on 18-day-old *N. benthamiana* cotyledons. 2 weeks later, young leaves were infiltrated with *A. tumefaciens* carrying the TYLCV infectious clone (WT or V2null) and leaf patches were collected at 3, 4, or 9 days post-inoculation (dpi).

B Experimental design for systemic TYLCV infection assays. *A. tumefaciens* carrying the TRV-EV or TRV-*NbAGO4* infectious clones were inoculated on 18-day-old *N. benthamiana* cotyledons. At the same time, *A. tumefaciens* carrying the TYLCV infectious clone (WT or V2null) were injected into plant stems. The top three leaves were collected at 3 weeks post-inoculation (wpi).

Figure S4. Original single-base resolution bisulfite sequencing data of the intergenic region (IR) of TYLCV in local infection assays at 3 dpi or 9 dpi (Figure 5A).

At least 5 individual clones were sequenced per replicate and sample at 3 dpi, and >18 individual were sequenced per replicate and sample at 9 dpi. Each single circle, corresponding to a cytosine, is colored in blue, red, or green, representing the CHG, CG or CHH contexts, respectively. Methylated cytosines are represented by filled circles, while unmethylated cytosines are represented by empty circles.

Figure S5. Original single-base resolution bisulfite sequencing data of the intergenic region (IR) of TYLCV-V2null in local infection assays at 4 dpi in *NbAGO4*-silenced plants (Figure 5B). At least 7 individual clones were sequenced per sample in the first replicate, and > 15 individual clones were sequenced per sample in replicates second to fourth. Each single circle,

corresponding to a cytosine, is colored in blue, red, or green, representing the CHG, CG or CHH contexts, respectively. Methylated cytosines are represented by filled circles, while unmethylated cytosines are represented by empty circles.

Figure S6. Original single-base resolution bisulfite sequencing data of the intergenic region (IR) of TYLCV and TYLCV-V2null in systemic infection assays in *NbAGO4*-silenced plants (Figure 5C).

> 14 individual clones were sequenced per sample and replicate. Each single circle, corresponding to a cytosine, is colored in blue, red, or green, representing the CHG, CG or CHH contexts, respectively. Methylated cytosines are represented by filled circles, while unmethylated cytosines are represented by empty circles.

Figure S7. TYLCV $V2_{L76S}$ interacts with AGO4 in the Cajal body.

A Alignment of the amino acid sequences of V2 from *Cotton Leaf Curl Multan virus* (CLCuMuV) and V2 from TYLCV. The alignment was performed by Geneious (https://www.geneious.com). Black background indicates conservation. The identity of these two proteins is 65%.

B $V2_{L76S}$-GFP and RFP-AGO4 co-localize in the Cajal body. CFP-Fibrillarin, $V2_{L76S}$-GFP and RFP-NbAGO4-1/2 or RFP-SlAGO4a/b/d were transiently co-expressed in *N. benthamiana* epidermal cells. CFP-Fibrillarin is used as a nucleolus and Cajal body marker. Confocal images were taken at two days after infiltration. Arrowheads indicate the position of the Cajal body. Bar, 5μm. This experiment was repeated three times with similar results.

C 3xHA-NbAGO4-1 interacts with V2-GFP and $V2_{L76S}$-GFP in co-immunoprecipitation (co-IP) assays upon transient expression in *N. benthamiana*. Free GFP was used as negative control. CBB, Coomassie brilliant blue staining. The V2-GFP sample was diluted 1/20 for western blot to reach a protein amount comparable to that of $V2_{L76S}$-GFP. Three independent biological replicates were performed with similar results.

D $V2_{L76S}$ interacts with AGO4 in the Cajal body. The N-terminal half of the YFP fused to $V2_{L76S}$ ($V2_{L76S}$-nYFP) was transiently co-expressed with the C-terminal half of the YFP alone (cYFP, as a negative control), or cYFP-NbAGO4, cYFP-SlAGO4, or cYFP- $V2_{L76S}$ in *N. benthamiana* leaves. CFP-Fibrillarin was used as a nucleolus and Cajal body marker. V2 was used as a

925 control. Yellow fluorescence indicates a positive interaction. Arrowheads indicate the position
926 of the Cajal body. Bar, 5μm. This experiment was repeated three times with similar results.

927

928 **Figure S8. Model for the V2-mediated inhibition of the AGO4-dependent methylation of the**
929 **viral DNA.**

930 During the viral infection, the ssDNA TYLCV genome forms dsDNA replicative intermediates,
931 which could be targeted by the host AGO4-dependent RNA-directed DNA methylation (RdDM)
932 pathway as an antiviral defence mechanism. Viral small interfering RNA (vsiRNA) are generated
933 and loaded into AGO4. In the absence of the virus-encoded V2 protein, the AGO4-vsiRNA
934 complex could be effectively guided towards the viral genome by complementary base pairing to
935 the scaffold RNA and association with Pol V, and recruit the methyl transferase DRM2 to catalyze
936 methylation of the viral genome. When V2 is present, however, V2 interacts with AGO4 and
937 interferes with the binding of this protein to the viral DNA, enabling viral evasion from the AGO4-
938 dependent DNA methylation.

Figure 1

A

Identified protein name	Identified protein ID	Bait protein name	Exclusive unique peptide count	Identified protein coverage (%)	Best Mascot Score
NbAGO4-1	NbS00018144g003.1	GFP	- / - / -	- / - / -	- / - / -
		V2-GFP	3 / - / -	6.1 / - / -	44.9 / - / -
NbAGO4-2	NbS00007950g0008.1	GFP	- / - / -	- / - / -	- / - / -
		V2-GFP	16 / 1 / 1	23 / 1.8 / 1.2	116.2 / 35.7 / 59.2

B

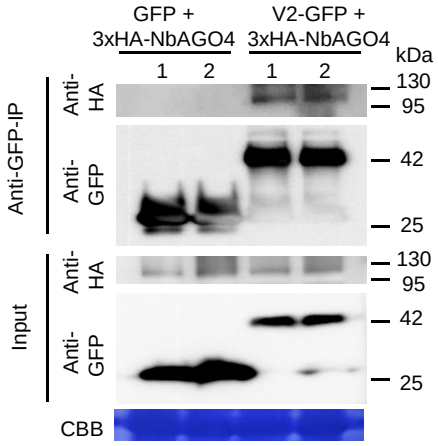

C

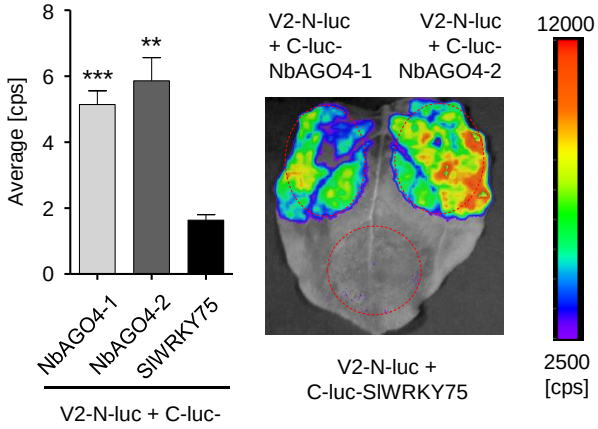

Figure 2

A

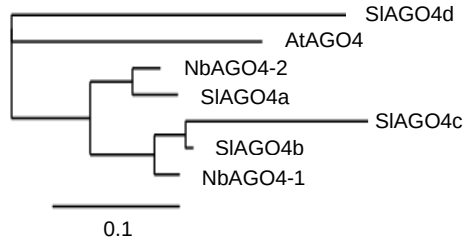

B

Identity (%) / Distance matrix

Distance / Identity	AtAGO 4	NbAGO 4-1	NbAGO 4-2	SlAGO 4a	SlAGO 4b	SlAGO 4c	SlAGO 4d
AtAGO4		0.302	0.303	0.305	0.308	0.390	0.384
NbAGO4-1	73.5		0.133	0.137	0.056	0.177	0.339
NbAGO4-2	73.4	86.8		0.071	0.148	0.242	0.329
SlAGO4a	73.5	86.8	92.5		0.140	0.248	0.336
SlAGO4b	73.0	94.4	85.4	86.4		0.146	0.332
SlAGO4c	67.3	83.1	77.7	77.6	85.7		0.432
SlAGO4d	67.8	70.8	71.6	71.1	71.2	64.9	

C

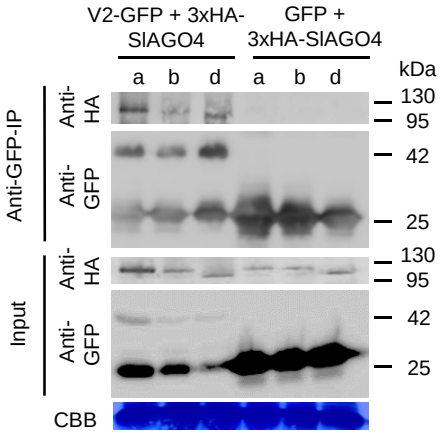

D

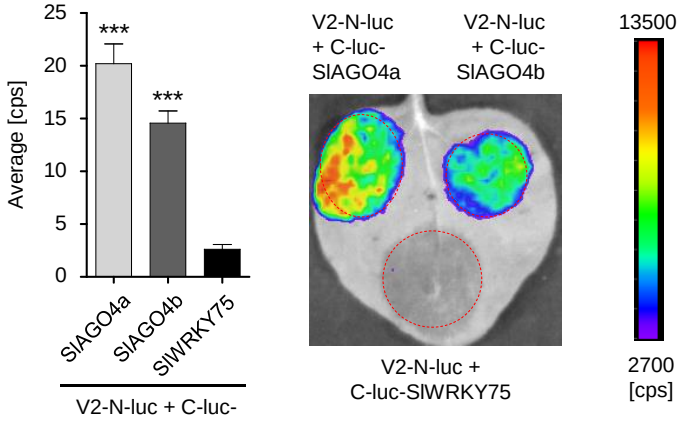

Figure 3

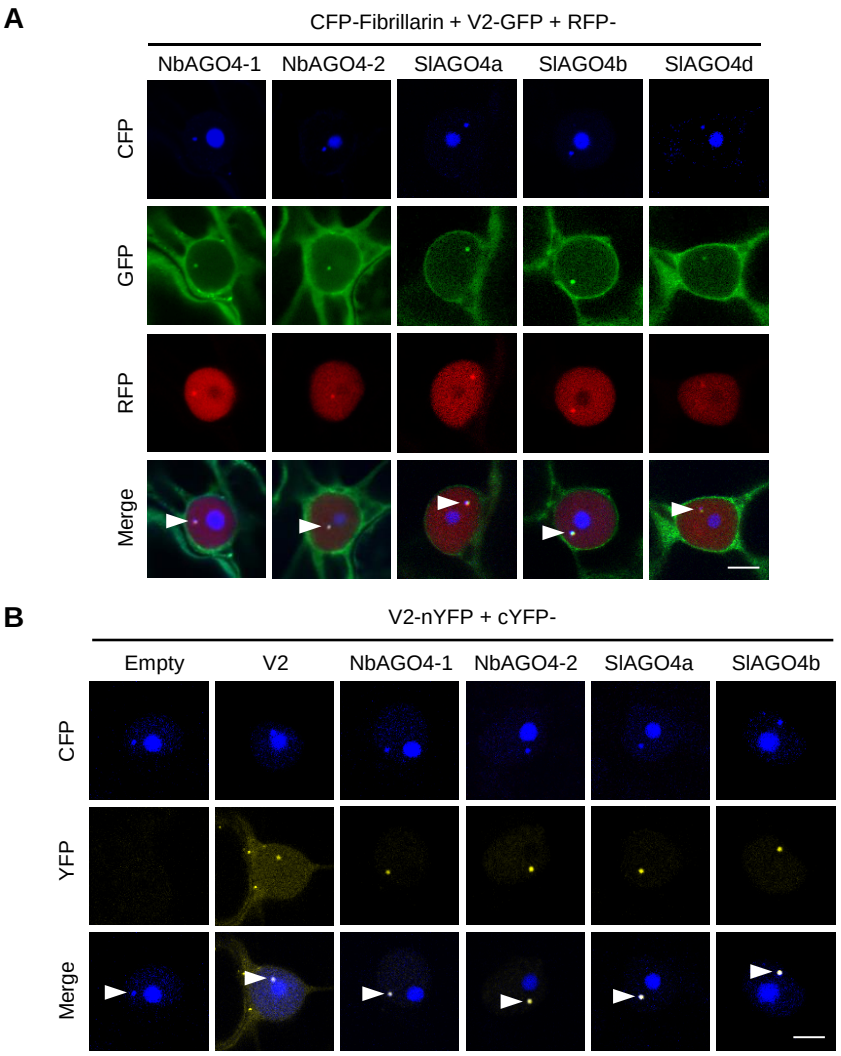

Figure 4

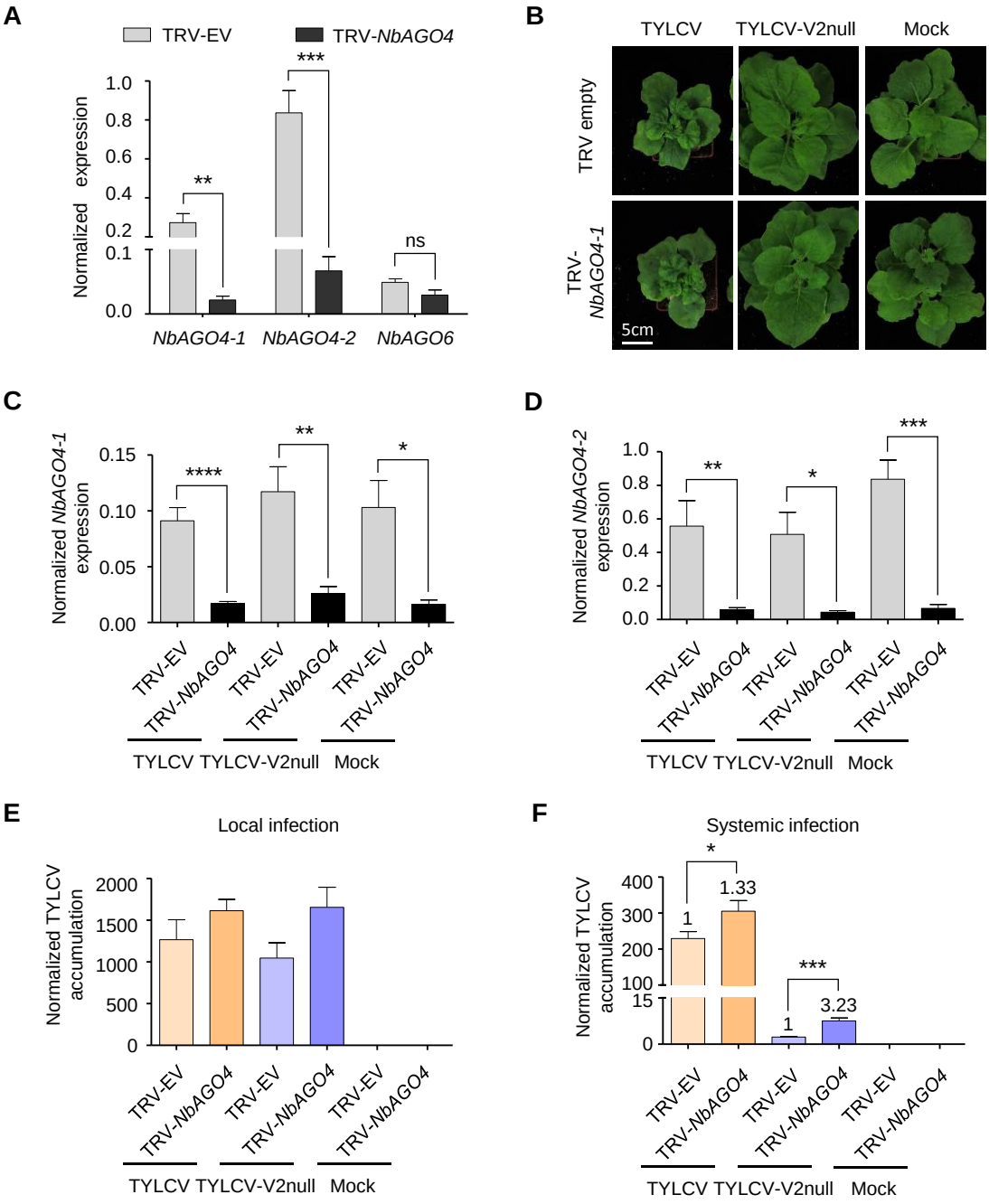

Figure 5

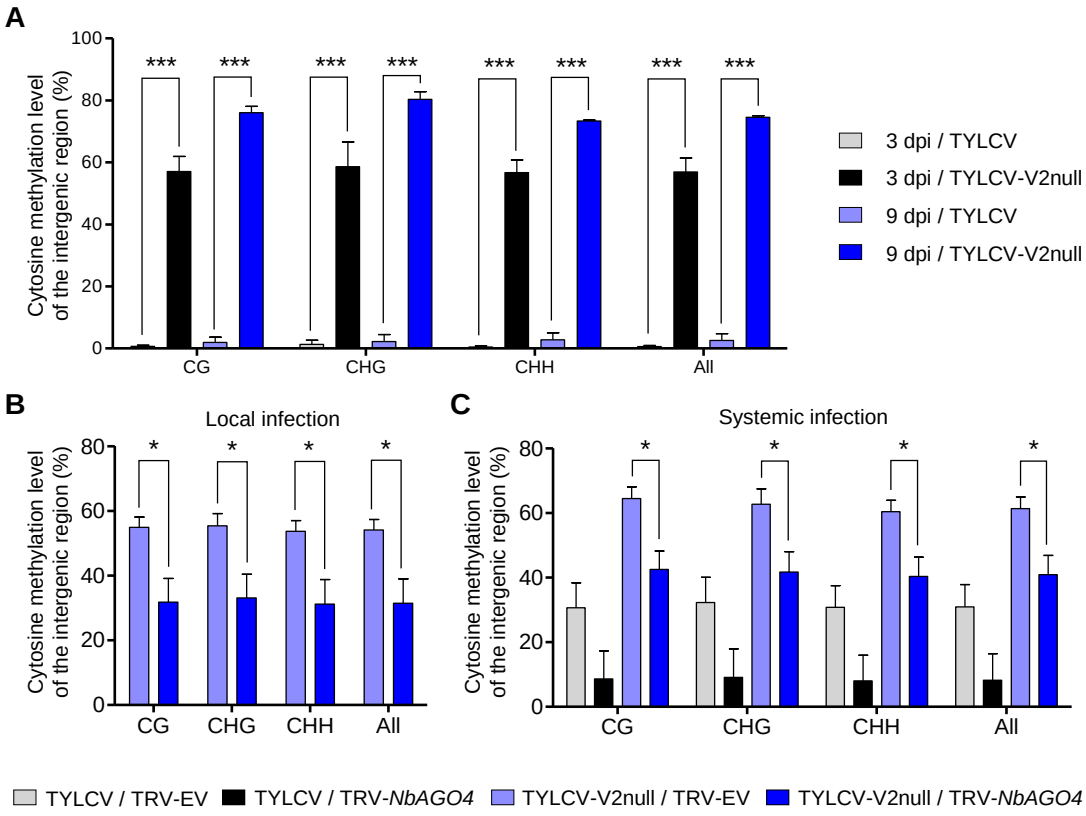

Figure 6